



# Diffusion kurtosis imaging with multiple quantitative parameters for predicting microsatellite instability status of endometrial carcinoma

Qingling Song<sup>1</sup> · Wan Dong<sup>2</sup> · Shifeng Tian<sup>1</sup> · Lizhi Xie<sup>3</sup> · Lihua Chen<sup>1</sup> · Qiang Wei<sup>1</sup> · Ailian Liu<sup>1</sup>

Received: 5 May 2023 / Revised: 28 August 2023 / Accepted: 29 August 2023 / Published online: 22 September 2023  
© The Author(s), under exclusive licence to Springer Science+Business Media, LLC, part of Springer Nature 2023

## Abstract

**Purpose** To explore the value of Diffusion kurtosis imaging (DKI) with multiple quantitative parameters in predicting microsatellite instability (MSI) status in endometrial carcinoma (EC).

**Methods** Data of 38 patients with EC were retrospectively analyzed, including 12 MSI and 26 microsatellite stability (MSS). All patients underwent preoperative 1.5T MR examination. The quantitative values of the DKI sequence in the tumor parenchyma of the two groups, including mean kurtosis (MK), axial kurtosis (Ka), radial kurtosis (Kr), fractional anisotropy (FA), fractional anisotropy of kurtosis (FAk), mean diffusivity (MD), axial diffusivity (Da), and radial diffusivity (Dr) were measured by two observers, respectively.

**Results** The MK, Ka, Kr, FA, FAk, MD, Da, and Dr values of the MSI group were  $1.074 \pm 0.162$ ,  $1.253 \pm 0.229$ ,  $0.886 \pm 0.205$ ,  $0.207 \pm 0.041$ ,  $0.397 \pm 0.129$ ,  $0.890 \pm 0.158 \mu\text{m}^2/\text{ms}$ ,  $1.083 \pm 0.218 \mu\text{m}^2/\text{ms}$ , and  $0.793 \pm 0.133 \mu\text{m}^2/\text{ms}$ , and  $0.956$  (0.889,1.002),  $1.048 \pm 0.211$ ,  $0.831 \pm 0.099$ ,  $0.188 \pm 0.061$ ,  $0.334$  (0.241,0.410),  $1.043 \pm 0.217 \mu\text{m}^2/\text{ms}$ ,  $1.235 \pm 0.229 \mu\text{m}^2/\text{ms}$ , and  $0.946 \pm 0.215 \mu\text{m}^2/\text{ms}$  in the MSS group. The MK and Ka values of the MSI group were higher than those of the MSS group ( $P < 0.05$ ), while the MD and Dr values were lower than those of the MSS group ( $P < 0.05$ ). The AUC of MK, Ka, MD, and Dr values in predicting MSI status of EC was 0.763, 0.729, 0.731, 0.748, respectively. The sensitivity was 58.3%, 50.0%, 65.4%, 61.5%, and the specificity was 96.2%, 92.3%, 75.0%, 83.3%, respectively.

**Conclusion** DKI can provide multiple quantitative parameters for predicting the MSI status of EC, and assist gynecologist to optimize the treatment plan for the patients.

**Keywords** Endometrial carcinoma · Microsatellite instability · Diffusion kurtosis imaging · Magnetic resonance imaging

Qingling Song and Wan Dong have contributed equally to this work.

✉ Ailian Liu  
liuailian@dmu.edu.cn

Qingling Song  
18698839975@163.com

Wan Dong  
291356027@qq.com

Shifeng Tian  
TSF253356@163.com

Lizhi Xie  
rokage@163.com

Lihua Chen  
yayachen428@yeah.net

Qiang Wei  
weiqiang@firsthosp-dmu.com

- <sup>1</sup> Department of Radiology, The First Affiliated Hospital of Dalian Medical University, Xigang district, Zhongshan road, No.222, Dalian 116011, China
- <sup>2</sup> Department of Radiology, Wuhan Children's Hospital, Tongji Medical College of Huazhong University of Science & Technology, Jiang'an District Wuhan Hong Kong Road No.100, Wuhan 430019, China
- <sup>3</sup> GE Healthcare, MR Research, Beijing 100024, China

## Introduction

Microsatellite instability (MSI), which results from the failure of *mismatch* repair (MMR) proteins to fix a *DNA replication* error, causes insertions, mismatches, or deletions during the DNA replication process, thus having an essential role in maintaining the stability of the genome and regulating gene expression [1–3]. MSI is considered as one of the pathogenesis of endometrial carcinoma (EC) [4]. Assessing the MSI status of EC can help evaluate cancer prognosis, judge the effect of immunosuppressive therapy, screen Lynch syndrome (LS) related cases [5, 6]. It provides a reasonable basis for the implementation of personalized precision treatment for patients with EC. Currently, immunohistochemistry is considered the most common method to determine the MSI status of EC, including the expression of four mismatch repair proteins in tumor tissues such as MLH-1, MSH-2, MSH-6, and PMS-2 [7]. Yet, this method is usually performed after surgery.

The detection of MSI status in EC has become crucial ever since anti-PD-1 monoclonal antibody pembrolizumab was authorized for the treatment of MSI solid tumors [8]. Immune checkpoint inhibitors might offer better clinical outcome over chemotherapy in frontline treatment for advanced endometrial cancer identified as MSI-high [9], thus, evaluation of MSI status is of importance to plan the therapy schema in the beginning. The MSI status has been more and more valued in clinical practice, and the National Comprehensive Cancer Network (NCCN) [10] and European Society for Medical Oncology (ESMO) [11] guidelines both have recommended testing MSI status in all EC patients.

The use of magnetic resonance imaging (MRI) related techniques can be used to predict the MSI status of EC before surgery. For example, Bhosale et al. have suggested that the standard ADC value and D value of intravoxel incoherent motion (IVIM) sequences within a small field of view (FOV) can reflect the MSI status of stage I EC [12]. Moreover, Ahmed et al. [13] found a higher T1 signal intensity ratio in EC patients with MSI compared to those with microsatellite stability (MSS). The diffusion kurtosis imaging (DKI) sequence is an extension of the diffusion-weighted imaging (DWI) and the diffusion tensor imaging (DTI) sequence. It is based on the non-Gaussian distribution model of water molecules. The DKI sequence can more accurately reflect the changes in the microenvironment in the tissue, quantify the deviation of water molecules caused by non-Gaussian dispersion [14–16], and provide multiple quantitative parameters.

This study aimed to explore the value of multiple quantitative parameters of DKI sequence in predicting MSI

status of EC to provide new ideas for non-invasive preoperative diagnosis in predicting MSI status and expanding the application of DKI sequence for uterine diseases.

## Materials and methods

### Patients

Data from patients with EC confirmed by surgical pathology were retrospectively analyzed from January 2018 to April 2020. The inclusion criteria were as follows: (1) primary EC confirmed by postoperative pathology; (2) MRI examination was performed in our hospital within 2 weeks before the surgery; the scanning sequences contained DKI; (3) no radiotherapy, chemotherapy, and other treatments (including curettage and biopsy) before the examination; (4) with complete pathological data, and the immunohistochemical analysis indexes included four proteins: MLH-1, MSH-2, MSH-6, and PMS-2. The expression of all four proteins was defined as MSS (any positive nuclear staining), otherwise, as MSI (negative nuclear staining of tumor cells). The exclusion criteria were as follows: (1) with drastic imaging artifact which affected the observation of the lesion and the data measurement; (2) the maximum diameter of the lesion was < 1.0 cm, which could not be clearly displayed in DKI derived parameter images or draw the regions of interest (ROIs).

This retrospective study was approved by the institutional review board, and informed consent was waived.

### Inspection method

The American GE Signa HDxt 1.5T MR superconducting scanner was used, with body 8-channel phased-array coils. The patients were placed in a supine position for scanning. Before the scan, patients refrained from eating, and they drank moderate water to fill the bladder. Also, patients wearing the birth control ring needed to remove the ring one day before the examination. The main scan sequence and parameter settings were as follows: axial T<sub>1</sub>WI sequence: TR/TE = 400/8.0 ms, matrix = 320 × 192, number of excitations (NEX) = 2.0, FOV = 40 cm × 40 cm, scanning time was about 1'40"; axial T<sub>2</sub>WI sequence: TR/TE = 4000/125 ms, matrix = 320 × 192, NEX = 4.0, FOV = 40 cm × 40 cm, scanning time was about 2'23"; axial DKI sequence: using single excited spin-echo plane echo (SE-EPI) sequence, TR/TE = 3000/98 ms, matrix = 128 × 128, NEX = 2.0, FOV = 32 cm × 32 cm, with 0, 1000 s/mm<sup>2</sup>, and 2000 s/mm<sup>2</sup> of b values. The diffusion gradient was applied in 30 orthogonal directions, and the scanning time was about 3'. The above sequence layer was 0.5 cm thick and 0.1 cm apart.

## Image analysis and data measurement

General information, such as the pathological type, pathological grade, and clinical stage of the lesion, were recorded by a radiologist (observer 1 with 5 years of MR diagnosis experience). The DKI image data were transmitted to the AW4.6 workstation (company information or cite related reference). Then, observer 1 and another radiologist (observer 2, with 10 years of MR diagnosis experience) completed the data measurement without knowing the patient's clinical and pathological diagnosis results. The workstation Function software package was used to post-process the original DKI images to obtain pseudo-color images of mean kurtosis (MK), axial kurtosis (Ka), radial kurtosis (Kr), and fractional anisotropy (FA), fractional anisotropy of kurtosis (FAk), mean diffusivity (MD), axial diffusivity (Da), and radial diffusivity (Dr) (Figs. 1, 2).

Referring to the  $T_2$ WI images, the largest section of the lesion and its upper and lower 1–2 levels were selected. The ROIs were manually drawn in the tumor parenchymal area. The ROIs encompassed as much solid area of the tumor as possible, avoiding the areas of necrosis, hemorrhage, and cystic degeneration (hyperintensity on  $T_2$ WI images) and appropriately avoiding the lesion's edge. Eight types of images could be arbitrarily switched when the ROIs were fixed, ensuring that the ROI could be placed on the same level and position of various pseudo-color images. The average value of ROI was taken as each DKI parameter value.

## Statistical analysis

SPSS 17.0 software was adopted for statistical analysis. Kolmogorov–Smirnov was used to test whether data conformed to the normal distribution. Those that accorded to the normal distribution were represented by  $x \pm s$ , and those that conformed to the skew distribution were represented by the median (P25, P75). The Chi-square test and Fisher exact test were used to compare the pathological types (high and low-risk) and clinical stages (early and late) of the two groups of cases. Intra-class correlation coefficients (ICC) were used to test the inter-reader agreement of the lesions' measurement results in two groups by the two observers.  $ICC < 0.40$  indicates poor inter-reader agreement,  $0.40 \leq ICC < 0.75$  indicates moderate agreement,  $ICC \geq 0.75$  means good agreement. The average of the results of two observers was taken for subsequent analysis. The independent-sample *t*-test (normal distribution) or *Mann-Whitney U* test (skew distribution) was used to compare the differences between the parameter values of the two groups. The difference was considered as statistically significant at  $P < 0.05$ . The receiver operator characteristic (ROC) curve was used to analyze the diagnostic efficiency

and the best diagnostic threshold of different parameters. The area under curve (AUC) was calculated, as well as the corresponding sensitivity and specificity.

## Results

### Patient characteristics

There were 38 patients (12 MSI cases and 26 MMS cases according to the immunohistochemical results) who were finally eligible for the study. The main clinical manifestations of premenopausal patients included increased menstrual flow and irregular menstruation; while that of postmenopausal patients included irregular vaginal bleeding.

The patient demographics and tumor characteristics of the study were shown in Table 1. Among the 12 MSI cases, the mean age was  $64.1 \pm 9.8$  years (range 47–82 years). There were five patients with high-risk tumor types (3 poorly differentiated endometrioid adenocarcinoma, 1 serous carcinoma, and 1 case of dedifferentiated carcinoma) and 7 patients with a low-risk type (6 moderately differentiated endometrioid adenocarcinoma and 1 well-differentiated endometrioid adenocarcinoma). Clinical stages included 8 early-stage (6 Ia stage, 2 Ib stage) cases and 4 advanced stage cases (1 II stage, 3 III stage) cases. There were 2 premenopausal patients and 10 postmenopausal patients.

Among the 26 cases of MMS, the mean age was  $56.7 \pm 12.8$  years (range 38–78 years). There were three patients with high-risk tumor types (2 poorly differentiated endometrioid adenocarcinoma, 1 serous carcinoma) and 23 low-risk tumor types (21 moderately differentiated endometrioid adenocarcinoma and 2 well-differentiated endometrioid adenocarcinomas). Clinical staging included 21 cases with an early-stage tumor (15 Ia stage, 6 Ib stage) and 5 cases with late-stage tumor (3 II stage, 2 III stage). There were 12 premenopausal patients and 14 postmenopausal patients.

There was no significant difference in age, tumor pathological type, clinical stages, and menopausal status between MMS and MSI groups, and the *P* value was 0.086, 0.081, 0.423, and 0.147, respectively.

### The inter-reader agreement test of the measurement results between the two observers

The inter-reader agreement test results of the parameters between the two groups by the two observers were shown in Table 2, and the inter-reader agreement of the data in each group was very good ( $ICC > 0.75$ ).

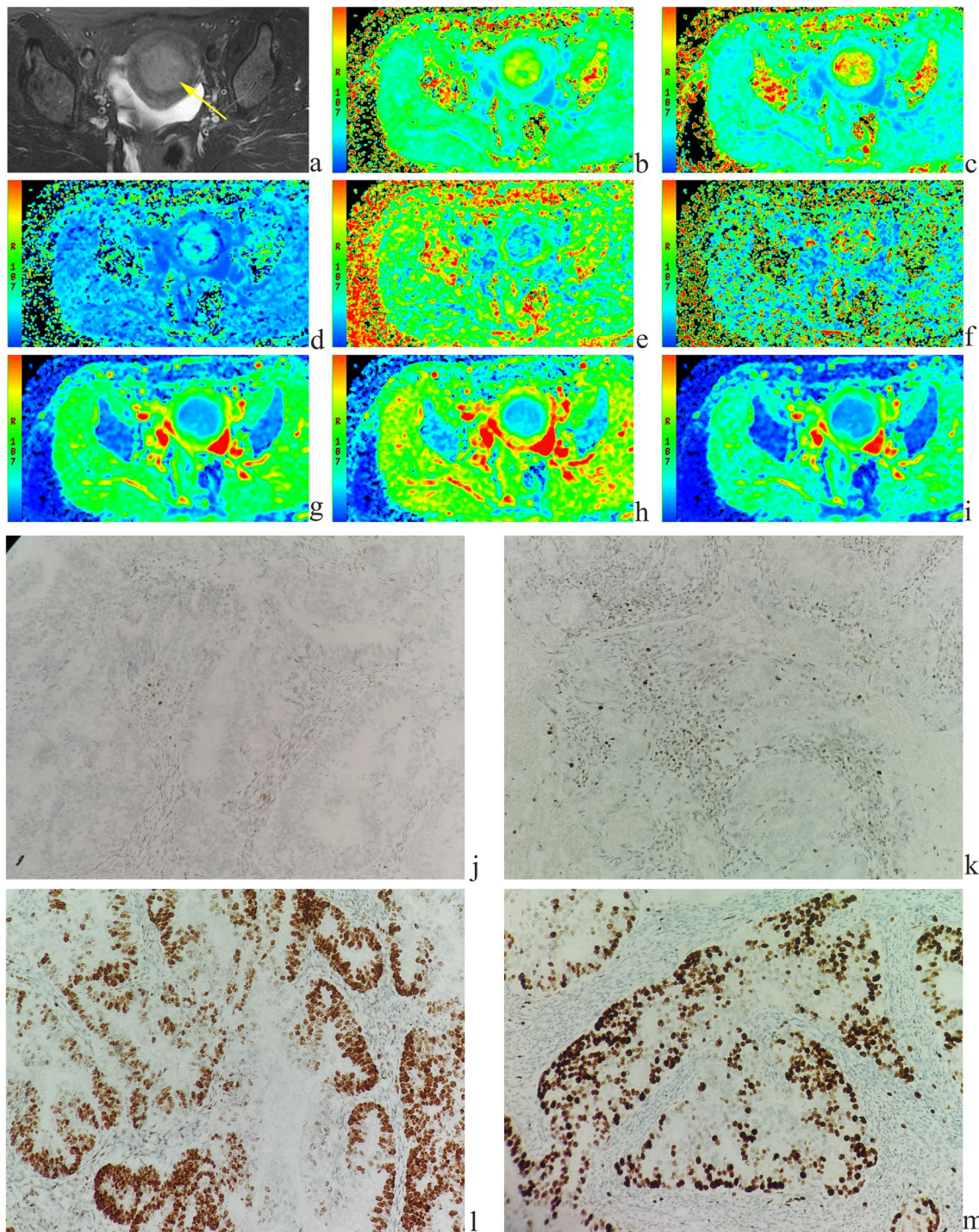


**Fig. 1** A 51-year-old patient with poorly differentiated EC. **a** The lesion is showed on T2WI (yellow arrow). **b–i** The pseudo-color images of MK, Ka, Kr, FA, FAK, MD, Da, and Dr of the DKI sequence. Their quantitative values are 1.295, 1.525, 1.115, 0.168,

0.355, 0.673  $\mu\text{m}^2/\text{ms}$ , 0.786  $\mu\text{m}^2/\text{ms}$ , and 0.616  $\mu\text{m}^2/\text{ms}$ , respectively. **j–m** Immunohistochemical staining, loss of expression of MLH-1 (**j**), loss of expression of PMS-2 (**k**), strong staining of MSH-2 (**l**), loss of expression of MSH-6 (**m**).

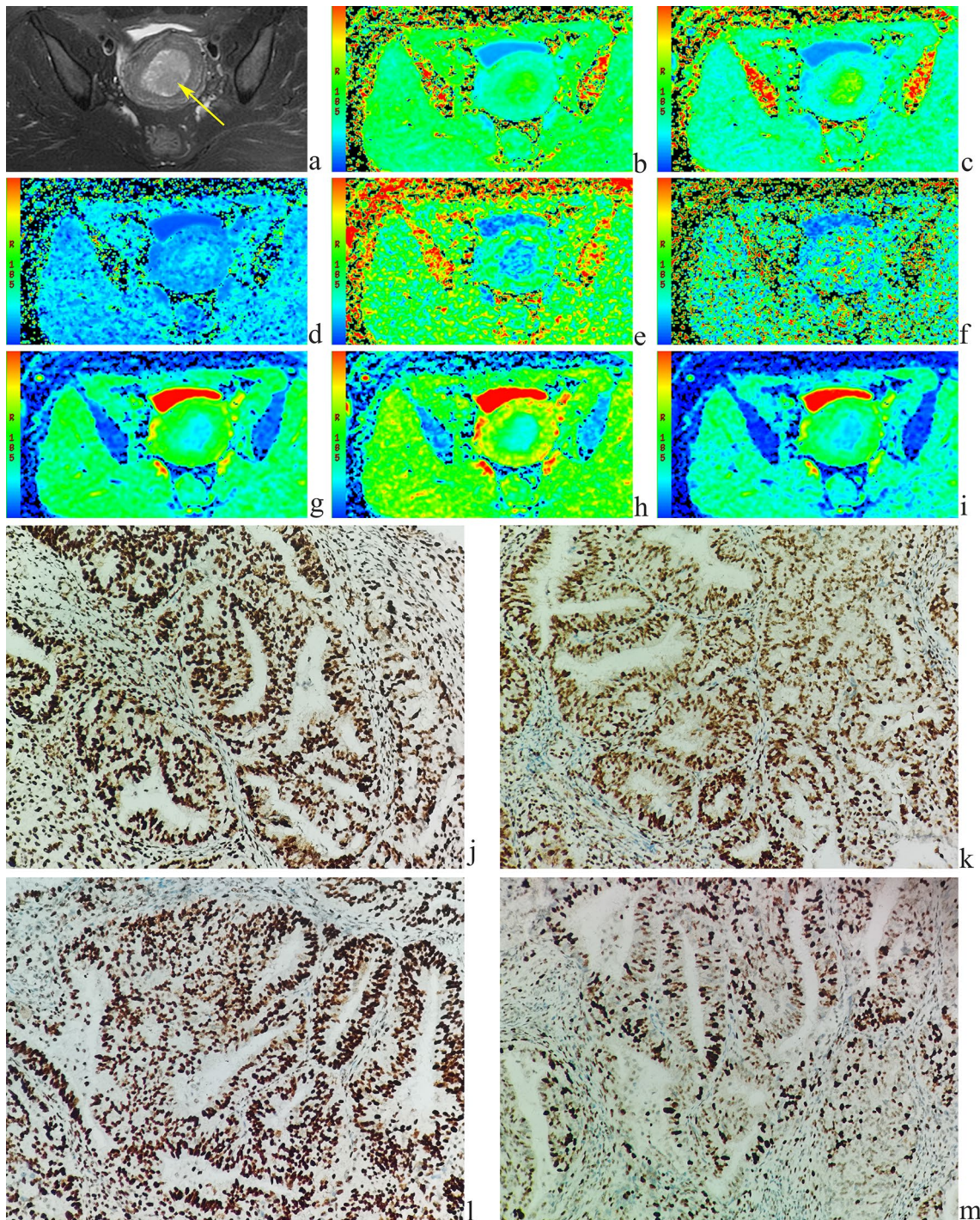


**Fig. 2** A 36-year-old patient with median-high differentiated EC. **a** The lesion is showed on T2WI (yellow arrow). **b–i** The pseudo-color images of MK, Ka, Kr, FA, FAk, MD, Da, and Dr of the DKI sequence. Their quantitative values are 0.903, 1.05, 0.791, 0.177,

0.337, 1.125  $\mu\text{m}^2/\text{ms}$ , 1.32  $\mu\text{m}^2/\text{ms}$ , and 1.024  $\mu\text{m}^2/\text{ms}$ , respectively. **j–m** Immunohistochemical staining, showing strong staining of MLH-1 (**j**), strong staining of PMS-2 (**k**), strong staining of MSH-2 (**l**), strong staining of MSH-6 (**m**).

**Table 1** Patient demographics and tumor characteristics

	MSI group (n = 12)	MSS group (n = 26)	P value
Age (years)	64.1 ± 9.8	56.7 ± 12.8	0.086
Tumor type			0.081
High-risk	5	3	
Low-risk	7	23	
Clinical stage*			0.423
Early-stage	8	21	
Advanced stage	4	5	
Menopausal status			0.147
Premenopausal	2	12	
Postmenopausal	10	14	

\*Early-stage includes Ia stage and Ib stage, advanced stage includes II stage and III stage

### Comparison of DKI parameters between the two groups

The parameter values and results comparison between the MSI group and the MSS group were shown in Table 3. The MD and Dr values of the MSI group were smaller than those in the MSS group, while the MK and Ka values were greater than those in the MSS group. The differences were statistically significant ( $P < 0.05$ ). There was no statistical difference in Kr, FA, FAK, and Da values between the two groups ( $P > 0.05$ ).

### Efficacy of various parameters to diagnose MSI of EC and their comparison results

The parameters of the DKI sequence to identify the AUC of the two groups, the threshold, sensitivity, and specificity of predicting MSI status of EC are shown in Table 4; the ROC curve is presented in Fig. 3.

**Table 2** The inter-reader agreement test results of each parameter measured by two observers

	MSI group (n=12)			MSS group (n=26)		
	Observer 1	Observer 2	ICC	Observer 1	Observer 2	ICC
MK	1.076 ± 0.148	1.072 ± 0.179	0.976	0.954 (0.865,0.993)	0.936 ± 0.128	0.938
Ka	1.244 ± 0.214	1.262 ± 0.249	0.970	1.040 ± 0.221	1.056 ± 0.210	0.956
Kr	0.890 ± 0.203	0.881 ± 0.209	0.986	0.824 ± 0.109	0.838 ± 0.106	0.823
FA	0.195 (0.171,0.216)	0.212 ± 0.039	0.935	0.178 (0.153,0.211)	0.188 ± 0.063	0.948
FAk	0.391 ± 0.126	0.403 ± 0.136	0.965	0.352 ± 0.156	0.336 ± 0.146	0.925
MD (µm <sup>2</sup> /ms)	0.881 ± 0.156	0.900 ± 0.165	0.973	1.042 ± 0.228	1.044 ± 0.221	0.933
Da (µm <sup>2</sup> /ms)	1.067 ± 0.220	1.099 ± 0.222	0.970	1.233 ± 0.245	1.237 ± 0.232	0.917
Dr (µm <sup>2</sup> /ms)	0.787 ± 0.128	0.800 ± 0.141	0.971	0.946 ± 0.224	0.947 ± 0.219	0.941

MSI microsatellite instability, MSS microsatellite stability, MK mean kurtosis, Ka axial kurtosis, Kr radial kurtosis, FA fractional anisotropy, FAK fractional anisotropy of kurtosis, MD mean diffusivity, Da axial diffusivity, Dr radial diffusivity, ICC intra-class correlation coefficients, ICC < 0.40 indicates poor inter-reader agreement, 0.40 ≤ ICC < 0.75 indicates moderate agreement, ICC ≥ 0.75 means good agreement;

**Table 3** The parameter values and results comparison between the two groups of cases

	MSI group (n=12)	MSS group (n=26)	Statistical value	P-value
MK	1.074 ± 0.162	0.956 (0.889,1.002)	- 2.576*	0.010
Ka	1.253 ± 0.229	1.048 ± 0.211	2.710	0.010
Kr	0.886 ± 0.205	0.831 ± 0.099	1.128	0.267
FA	0.207 ± 0.041	0.188 ± 0.061	0.987	0.330
FAk	0.397 ± 0.129	0.334 (0.241, 0.410)	- 1.131*	0.258
MD (µm <sup>2</sup> /ms)	0.890 ± 0.158	1.043 ± 0.217	- 2.178	0.036
Da (µm <sup>2</sup> /ms)	1.083 ± 0.218	1.235 ± 0.229	- 1.933	0.061
Dr (µm <sup>2</sup> /ms)	0.793 ± 0.133	0.946 ± 0.215	- 2.261	0.030

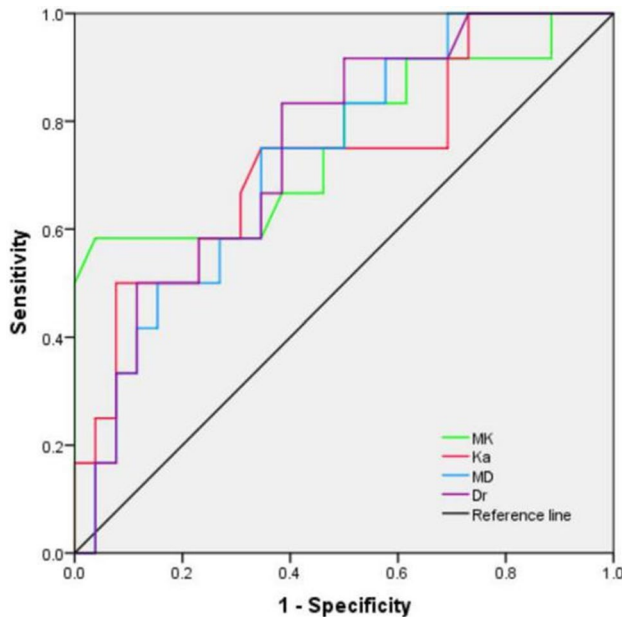
MSI microsatellite instability, MSS microsatellite stability, MK mean kurtosis, Ka axial kurtosis, Kr radial kurtosis, FA fractional anisotropy, FAK fractional anisotropy of kurtosis, MD mean diffusivity, Da axial diffusivity, Dr radial diffusivity.

\*is Z value, the rest is t value, Significant correlation at 0.05 levels

**Table 4** AUC, threshold, sensitivity, and specificity of each parameter

	AUC (95% confidence interval)	Threshold	Sensitivity (%)	Specificity (%)
MK	0.763 (0.579 ~ 0.946)	1.078	58.3	96.2
Ka	0.729 (0.550 ~ 0.909)	1.298	50.0	92.3
MD	0.731 (0.566 ~ 0.896)	0.992 $\mu\text{m}^2/\text{ms}$	65.4	75.0
Dr	0.748 (0.588 ~ 0.909)	0.891 $\mu\text{m}^2/\text{ms}$	61.5	83.3

AUC area under the curve, MK mean kurtosis, Ka axial kurtosis, MD mean diffusivity, Dr radial diffusivity.

**Fig. 3** ROC curve of MK, Ka, MD, and Dr value for predicting MSI status of EC. AUC is 0.763, 0.729, 0.731, and 0.748, respectively.

## Discussion

Microsatellite instability (MSI) is one of the criteria for molecular classification of EC by the Cancer Genome Atlas (TCGA) [17]. Prediction of MSI status before surgery can predict patients' prognosis with EC more accurately, thus providing a basis for the subsequent traditional adjuvant therapy or the introduction of future immune and targeted therapy.

MSI is closely related to the occurrence of Lynch syndrome (LS). Patients with LS have a significantly increased risk of developing colorectal cancer, ovarian cancer, and EC. EC usually occurs before other tumors and is considered the "sentinel Cancer" of LS patients. [18, 19]. Therefore, close monitoring of patients with MSI status of EC diagnosed with LS may contribute to early detection, prevention, and treatment of other related cancers.

In evaluating the curative effect, relevant clinical studies have shown that tumors expressing PD-L1a have a significant response to PD-1/PD-L1 immunotherapy. The

expression level of PD-L1 protein in MSI tumors is significantly higher than that in MSS tumors [20]. Therefore, it is believed that by evaluating MSI status in EC patients, doctors might accurately predict the clinical efficacy of PD-1/PD-L1 immunotherapy. Yet, the relationship between MSI and the prognosis of EC is still controversial. Some studies advocate that EC with MSI status may have a higher pathological grade, deeper myometrial invasion, and a greater possibility of involvement of cervical and lymph nodes [21], thus suggesting poor prognosis. Nevertheless, other studies propose that MSI is an indicator of EC's good prognosis [22]. The inconsistencies between those studies may be related to the small sample size, the difference in detection methods of MSI, as well as the difference in the number of microsatellites analyzed and the number of specific sites selected. Overall, there is a certain correlation between MSI status and the prognosis of EC.

DKI is a non-enhanced MR imaging that does not require contrast agents. It can be used to accurately reflect the non-Gaussian distribution and diffusion state of water molecules in biological tissues and the microstructure's complexity of the tissue [23]. The application of the DKI sequence to EC has been previously reported. Yamada et al. [24] found that the MK and MD values of the DKI sequence can quantitatively evaluate deep myometrial infiltration and lymph node metastasis of EC and have a certain correlation with the histological grade of EC. Yue et al. [25] compared the differences between DWI and DKI sequence parameters in distinguishing histological grading of EC and found that compared with DWI sequence, the mathematical model of DKI sequence was more complete, and the parameters were more sensitive. In other studies, DKI histogram analysis was used to evaluate the depth of myometrial invasion, histological grade, and lymph node metastasis of EC [26, 27], the results suggested that the histogram of DKI parameters were able to predict the deep myometrial invasion, identified metastatic lymph node, evaluate tumor grade, and reached a satisfied performance.

The use of quantitative parameters of DKI sequence to assess MSI status in EC has not yet been reported. In this study, the inter-reader agreement of data measurement in each group was very good (ICC > 0.75), thus suggesting that DKI parameters' measurement is highly repeatable and stable.

The MK value is a representative parameter of the DKI sequence, representing the average value of diffusion kurtosis in all spatial directions [28]. It does not depend on the spatial orientation of the tissue structure and can truly reflect the degree of deviation between the diffusion displacement of water molecules in Gaussian distribution and the diffusion displacement of real water molecules in the tissue. Its magnitude is positively correlated with the complexity of the organizational structure in the ROI [29]. The Ka value represents the average kurtosis value along the diffusion tensor's long axis, and the Kr value represents the average kurtosis value perpendicular to the long axis of the diffusion tensor [30]. Both of them are also proportional to tissue complexity. Our results showed that the MK and Ka values of EC in the MSI group ( $1.074 \pm 0.162$ ,  $1.253 \pm 0.229$ ) were higher than those in the MSS group ( $0.956$  ( $0.889, 1.002$ ),  $1.048 \pm 0.211$ ). Previous studies have suggested more lymphocytic infiltration [31] and undifferentiated compound accumulation [32] in tumor tissues of MSI-related EC, which may increase the microenvironment's complexity diffusion of water molecules. In addition, the results of Travaglino et al. [33] suggested that the frequency of high-risk pathological cases in MSI-related EC was higher, which is consistent with the results of this study. The high-risk pathological type of EC has more active tumor cell proliferation, more vigorous tumor growth, and more abundant neovascularization [34, 35], which further increase the microenvironment's heterogeneity and complexity for water molecule diffusion in MSI-related EC.

The traditional ADC value is based on the assumption that water diffusion follows Gaussian behavior, that is, water molecules can diffuse without any restriction. However, in alive tissue, diffusion is usually limited by the microstructure of the organization, which means it exhibits a non-Gaussian phenomenon [36]. The parameter diffusion rate of non-Gaussian diffusion distribution theory can reflect the diffusion of water molecules in tumor tissues. MD value is the ADC value corrected by non-Gaussian distribution, reflecting the diffusion level and diffusion resistance of the molecule, so it is more accurate to express the movement of water molecules in living tissues [37]. Da value represents the diffusion coefficient of water molecules in the main diffusion direction, and Dr value the average of all diffusion coefficients perpendicular to the main diffusion direction. Both of them are proportional to the degree of freedom of movement in water molecules [38]. In this study, the MD and Dr values in the MSI group were lower than those of the MSS group. As the activity and ability of tumor cell proliferation of MSI-related EC are higher than that of MSS-related EC, and there are more lymphocytes and other substances infiltrating tumor tissue, it is speculated that the tumor cells of MSI-related EC are more compactly arranged, the extracellular space is smaller, and the degree of water molecule

diffusion is more restricted, which can lead to the decrease of MD and Dr values. Bhosale et al. [12] used small-field IVIM to predict the MSI status of stage I EC and found that the ADC value of MSI-related EC ( $0.787 \times 10^{-3} \text{mm}^2/\text{s}$ ) was lower than that of MSS ( $1.021 \times 10^{-3} \text{mm}^2/\text{s}$ ), which was similar to the results of this study.

The FA value reflects the degree of anisotropy of the movement of water molecules in the tissue. It is closely related to the integrity of the tissue fiber bundle and the consistency of the direction [39]. The FAK value is similar to the FA value, representing the anisotropy between the diffusion kurtosis values in the three axial directions of the diffusion tensor [40]. In this study, there was no significant difference in FA and FAK values between the two groups. Similar results were obtained in previous studies on evaluating low-grade glioma and the prediction of survival of high-grade gliomas by DKI [41, 42]. The value of FA and FAK in evaluating the MSI status of EC needs to be further explored. At the same time, it should be pointed out that the values of MK, Ka, MD, and Dr in this study are moderately effective in predicting MSI status of EC ( $0.7 < \text{AUC} < 0.8$ ), with low sensitivity but high specificity, mainly due to the small number of cases.

This study has a few limitations. First, the number of cases is relatively small (especially the MSI group). In addition, no further grouping was made according to tumor stage, pathological grade, and classification, which may cause bias in some results. The above factors might impede to accurately assess the performance of DKI parameters in predicting the MS status in EC. However, as a preliminary study, the results of this study revealed the potential of DKI parameters to be a non-invasive method for preoperative detection of MSI status, which is of great clinical significance. Moreover, a further multicenter study with larger cohort or a prospective study is warrant, that investigate and verify the value of DKI parameters in the prediction of MS status of EC in different groups of histologic feature and different clinical characteristics. Second, the ROIs were placed in the parenchymal area of EC, which may ignore part of the tumor heterogeneity information because it does not contain the entire area. Previous studies also commonly adopted this ROIs placement method, however, whole tumor region may provide more information. Therefore, the ROIs should include the whole tumor areas in the further study, and the texture of DKI images should be analyzed.

In conclusion, as non-enhanced functional imaging of MR, DKI can provide multiple quantitative parameters for non-invasive prediction of MSI status of EC, such as MK, Ka, MD, and Dr. As a non-invasive examination, DKI enables the patient to avoid the collateral injury caused by biopsy. Furthermore, DKI exam can obtain the timely results preoperatively instead of waiting for pathologic



confirmation. For the patients evaluated as suspected MSI could receive the timely specific therapy targeting the MSI to enhance the prognosis, that can provide the important reference for gynecologist to develop the optimal treatment plan and monitor the MSI status.

**Author contributions** Guarantor of integrity of the entire study: AL, QS, WD, ST. Study concepts and design: AL, QS, WD, ST, LC. Literature research: QS, WD, ST, AL. Clinical studies: QS, WD, ST, AL. Experimental studies/data analysis: QS, WD, ST, QW. Statistical analysis: QS, WD, ST, LX. Manuscript preparation: QS, WD, ST, LC, AL. Manuscript editing: QS, WD, ST, LX, QW, AL.

**Funding** No funding was received for this study.

## Declarations

**Conflict of interest** The authors have no relevant financial or non-financial interests to disclose.

**Ethical approval** The study was approved by the Ethics Committee of The First Affiliated Hospital of Dalian Medical University.

**Informed consent** Informed consent was obtained from all individual participants included in the study.

**Consent to participate** Informed consent was waived.

**Consent for publication** Not applicable.

## References

- Tamura K, Kaneda M, Futagawa M, Takeshita M, Kim S, Nakama M, Kawashita N, Tatsumi-Miyajima J (2019) Genetic and genomic basis of the mismatch repair system involved in Lynch syndrome. *Int J Clin Oncol. Sep*;24(9):999-1011. doi: <https://doi.org/10.1007/s10147-019-01494-y>.
- Kane AM, Fennell LJ, Liu C, Borowsky J, McKeone DM, Bond CE, Kazakoff S, Patch AM, Koufariotis LT, Pearson J, Waddell N, Leggett BA, Whitehall VLJ (2020) Alterations in signaling pathways that accompany spontaneous transition to malignancy in a mouse model of BRAF mutant microsatellite stable colorectal cancer. *Neoplasia. Feb*;22(2):120-128. doi: <https://doi.org/10.1016/j.neo.2019.12.002>.
- Greenberg A, Kariv R, Solar I, Hershkovitz D (2020) Geographic Heterogeneity for Mismatch Repair Proteins Is Associated with Defects in DNA Repair. *Isr Med Assoc J. Jan*;22(1):32-36. PMID: 31927803.
- Brooks RA, Fleming GF, Lastra RR, Lee NK, Moroney JW, Son CH, Tatebe K, Veneris JL (2019) Current recommendations and recent progress in endometrial cancer. *CA Cancer J Clin. Jul*;69(4):258-279. doi: <https://doi.org/10.3322/caac.21561>.
- Wadee R, Grayson W (2019) A potpourri of pathogenetic pathways in endometrial carcinoma with a focus on Lynch Syndrome. *Ann Diagn Pathol. Apr*;39:92-104. doi: <https://doi.org/10.1016/j.anndiagpath.2019.02.003>
- Luchini C, Bibeau F, Ligtenberg MJL, Singh N, Nottegar A, Bosse T, Miller R, Riaz N, Douillard JY, Andre F, Scarpa A (2019) ESMO recommendations on microsatellite instability testing for immunotherapy in cancer, and its relationship with PD-1/PD-L1 expression and tumour mutational burden: a systematic review-based approach. *Ann Oncol. Aug* 1;30(8):1232-1243. doi: <https://doi.org/10.1093/annonc/mdz116>.
- Timmerman S, Van Rompuy AS, Van Gorp T, Vanden Bempt I, Brems H, Van Nieuwenhuysen E, Han SN, Neven P, Victoor J, Laenen A, Vergote I (2020) Analysis of 108 patients with endometrial carcinoma using the PROMISE classification and additional genetic analyses for MMR-D. *Gynecol Oncol. Apr*;157(1):245-251. doi: <https://doi.org/10.1016/j.ygyno.2020.01.019>.
- Silveira AB, Bidard FC, Kasperek A, Melaabi S, Tanguy ML, Rodrigues M, Bataillon G, Cabel L, Buecher B, Pierga JY, Proudhon C, Stern MH (2020) High-Accuracy Determination of Microsatellite Instability Compatible with Liquid Biopsies. *Clin Chem*; 66:606-13. doi: <https://doi.org/10.1093/clinchem/hvaa013>.
- Hill BL, Graf RP, Shah K, Danziger N, Lin DI, Quintanilha J, Li G, Haberberger J, Ross JS, Santin AD, Slomovitz B, Elvin JA, Eskander RN (2023) Mismatch repair deficiency, next-generation sequencing-based microsatellite instability, and tumor mutational burden as predictive biomarkers for immune checkpoint inhibitor effectiveness in frontline treatment of advanced stage endometrial cancer. *Int J Gynecol Cancer. Apr* 3;33(4):504-513. doi: <https://doi.org/10.1136/ijgc-2022-004026>
- Abu-Rustum NR, Yashar CM, Bradley K et al (2021) NCCN Guidelines® insights: uterine neoplasms, version 3.2021. *J Natl Compr Canc Netw* 19:888–895. doi: <https://doi.org/10.6004/jnccn.2021.0038>
- Concin N, Matias-Guiu X, Vergote I et al (2021) ESGO/ESTRO/ESP guidelines for the management of patients with endometrial carcinoma. *Int J Gynecol Cancer* 31:12–39. doi: <https://doi.org/10.1136/ijgc-2020-002230>
- Bhosale P, Ramalingam P, Ma J, Iyer R, Soliman P, Frumovitz M, Kundra V (2017) Can reduced field-of-view diffusion sequence help assess microsatellite instability in FIGO stage I endometrial cancer? *J Magn Reson Imaging. Apr*;45(4):1216-1224. doi: <https://doi.org/10.1002/jmri.25427>.
- Ahmed M, Al-Khafaji JF, Class CA, Wei W (2018) Ramalingam P, Wakkaa H, Soliman PT, Frumovitz M, Iyer RB, Bhosale PR. Can MRI help assess aggressiveness of endometrial cancer? *Clin Radiol. Sep*;73(9):833.e11-833.e18. doi: <https://doi.org/10.1016/j.crad.2018.05.002>.
- Haopeng P, Xuefei D, Yan R, Zhenwei Y, Wei H, Ziyin W, Qungang S, Chaojie L, Linyan Y, Zhongmin W, Xiaoyuan F (2020) Diffusion kurtosis imaging differs between primary central nervous system lymphoma and high-grade glioma and is correlated with the diverse nuclear-to-cytoplasmic ratio: a histopathologic, biopsy-based study. *Eur Radiol. Apr*;30(4):2125-2137. doi: <https://doi.org/10.1007/s00330-019-06544-7>.
- Bickelhaupt S, Jaeger PF, Laun FB, Lederer W, Daniel H, Kuder TA, Wuesthof L, Paech D, Bonekamp D, Radbruch A, Delorme S, Schlemmer HP, Steudle FH, Maier-Hein KH (2018) Radiomics Based on Adapted Diffusion Kurtosis Imaging Helps to Clarify Most Mammographic Findings Suspicious for Cancer. *Radiology. Jun*;287(3):761-770. doi: <https://doi.org/10.1148/radiol.2017170273>.
- Yoon JH, Lee JM, Lee KB, Kim D, Kabasawa H, Han JK (2019) Comparison of monoexponential, intravoxel incoherent motion diffusion-weighted imaging and diffusion kurtosis imaging for assessment of hepatic fibrosis. *Acta Radiol. Dec*;60(12):1593-1601. doi: <https://doi.org/10.1177/0284185119840219>.
- Abdulfatah E, Wakeling E, Sakr S, Al-Obaidy K, Bandyopadhyay S, Morris R, Feldman G, Ali-Fehmi R (2019) Molecular classification of endometrial carcinoma applied to endometrial biopsy specimens: Towards early personalized patient management. *Gynecol Oncol. Sep*;154(3):467-474. doi: <https://doi.org/10.1016/j.ygyno.2019.06.012>.

18. Ryan N, Wall J, Crosbie EJ, Arends M, Bosse T, Arif S, Faruqi A, Frayling I, Ganesan R, Hock YL, McMahon R, Manchanda R, McCluggage WG, Mukonoweshuro P, van Schalkwyk G, Side L, Smith JH, Tanchel B, Evans DG, Gilks CB, Singh N (2019) Lynch syndrome screening in gynaecological cancers: results of an international survey with recommendations for uniform reporting terminology for mismatch repair immunohistochemistry results. *Histopathology*. Dec;75(6):813-824. doi: <https://doi.org/10.1111/his.13925>.
19. Kahn RM, Gordhandas S, Maddy BP, Baltich Nelson B, Askin G, Christos PJ, Caputo TA, Chapman-Davis E, Holcomb K, Frey MK (2019) Universal endometrial cancer tumor typing: How much has immunohistochemistry, microsatellite instability, and MLH1 methylation improved the diagnosis of Lynch syndrome across the population? *Cancer*. Sep 15;125(18):3172-3183. doi: <https://doi.org/10.1002/cncr.32203>.
20. Yang G, Zheng RY, Jin ZS (2019) Correlations between microsatellite instability and the biological behaviour of tumours. *J Cancer Res Clin Oncol*. Dec;145(12):2891-2899. doi: <https://doi.org/10.1007/s00432-019-03053-4>.
21. Ruz-Caracuel I, Ramón-Patino JL, López-Janeiro Á, Yébenes L, Berjón A, Hernández A, Gallego A, Heredia-Soto V, Mendiola M, Redondo A, Peláez-García A, Hardisson D (2019) Myoinvasive Pattern as a Prognostic Marker in Low-Grade, Early-Stage Endometrioid Endometrial Carcinoma. *Cancers (Basel)*. Nov 22;11(12):1845. doi: <https://doi.org/10.3390/cancers11121845>.
22. Dietmaier W, Büttner R, Rüschoff J. *Mikrosatelliteninstabilität: Aktueller Überblick über Methoden und Anwendungen* (2019) [Microsatellite instability: Review of methods and applications]. *Pathologie*. May;40(3):313-327. German. doi: <https://doi.org/10.1007/s00292-019-0610-7>.
23. Granata V, Fusco R, Setola SV, Palaia R, Albino V, Piccirillo M, Grimm R, Petrillo A, Izzo F (2019) Diffusion kurtosis imaging and conventional diffusion weighted imaging to assess electrochemotherapy response in locally advanced pancreatic cancer. *Radiol Oncol*. Jan 19;53(1):15-24. doi: <https://doi.org/10.2478/raon-2019-0004>.
24. Yamada I, Sakamoto J, Kobayashi D, Miyasaka N, Wakana K, Oshima N, Wakabayashi A, Saida Y, Tateishi U, Eishi Y (2019) Diffusion kurtosis imaging of endometrial carcinoma: Correlation with histopathological findings. *Magn Reson Imaging*. Apr;57:337-346. doi: <https://doi.org/10.1016/j.mri.2018.12.009>.
25. Yue W, Meng N, Wang J, Liu W, Wang X, Yan M, Han D, Cheng J (2019) Comparative analysis of the value of diffusion kurtosis imaging and diffusion-weighted imaging in evaluating the histological features of endometrial cancer. *Cancer Imaging*. Feb 14;19(1):9. doi: <https://doi.org/10.1186/s40644-019-0196-6>.
26. Chen T, Li Y, Lu SS, Zhang YD, Wang XN, Luo CY, Shi HB (2017) Quantitative evaluation of diffusion-kurtosis imaging for grading endometrial carcinoma: a comparative study with diffusion-weighted imaging. *Clin Radiol*. Nov;72(11):995.e11-995.e20. doi: <https://doi.org/10.1016/j.crad.2017.07.004>.
27. Song JC, Lu SS, Zhang J, Liu XS, Luo CY, Chen T (2020) Quantitative assessment of diffusion kurtosis imaging depicting deep myometrial invasion: a comparative analysis with diffusion-weighted imaging. *Diagn Interv Radiol*. Mar;26(2):74-81. doi: <https://doi.org/10.5152/dir.2019.18366>.
28. Tan Y, Zhang H, Wang X, Qin J, Wang L, Yang G, Yan H (2019) Comparing the value of DKI and DTI in detecting isocitrate dehydrogenase genotype of astrocytomas. *Clin Radiol*. Apr;74(4):314-320. doi: <https://doi.org/10.1016/j.crad.2018.12.004>.
29. Hempel JM, Brendle C, Bender B, Bier G, Kraus MS, Skardelly M, Richter H, Eckert F, Schittenhelm J, Ernemann U, Klose U (2019) Diffusion kurtosis imaging histogram parameter metrics predicting survival in integrated molecular subtypes of diffuse glioma: An observational cohort study. *Eur J Radiol*. Mar;112:144-152. doi: <https://doi.org/10.1016/j.ejrad.2019.01.014>.
30. Mastropietro A, Rizzo G, Fontana L, Figini M, Bernardini B, Straffi L, Marcheselli S, Ghirmai S, Nuzzi NP, Malosio ML, Grimaldi M (2019) Microstructural characterization of corticospinal tract in subacute and chronic stroke patients with distal lesions by means of advanced diffusion MRI. *Neuroradiology*. Sep;61(9):1033-1045. doi: <https://doi.org/10.1007/s00234-019-02249-2>.
31. Akhtar M, Al Hyassat S, Elaiwy O, Rashid S, Al-Nabet ADMH (2019) Classification of Endometrial Carcinoma: New Perspectives Beyond Morphology. *Adv Anat Pathol*. Nov;26(6):421-427. doi: <https://doi.org/10.1097/PAP.0000000000000251>.
32. Doghri R, Houcine Y, Boujelbène N, Driss M, Charfi L, Abbas I, Mrad K, Sellami R (2019) Mismatch Repair Deficiency in Endometrial Cancer: Immunohistochemistry Staining and Clinical Implications. *Appl Immunohistochem Mol Morphol*. Oct;27(9):678-682. doi: <https://doi.org/10.1097/PAI.0000000000000641>.
33. Travaglino A, Raffone A, Stradella C, Esposito R, Moretta P, Gallo C, Orlandi G, Insabato L, Zullo F (2020) Impact of endometrial carcinoma histotype on the prognostic value of the TCGA molecular subgroups. *Arch Gynecol Obstet*. Jun;301(6):1355-1363. doi: <https://doi.org/10.1007/s00404-020-05542-1>.
34. iang JX, Zhao JL, Zhang Q, Qing JF, Zhang SQ, Zhang YM, Wu XH (2018) Endometrial carcinoma: diffusion-weighted imaging diagnostic accuracy and correlation with Ki-67 expression. *Clin Radiol*. Apr;73(4):413.e1-413.e6. doi: <https://doi.org/10.1016/j.crad.2017.11.011>.
35. Tian S, Liu A, Zhu W, Li Y, Chen L, Chen A, Shen J, Song Q, Wei Q (2017) Difference in Diffusion-Weighted Magnetic Resonance Imaging and Diffusion Tensor Imaging Parameters Between Endometrioid Endometrial Adenocarcinoma and Uterine Serous Adenocarcinoma: A Retrospective Study. *Int J Gynecol Cancer*. Oct;27(8):1708-1713. doi: <https://doi.org/10.1097/IGC.00000000000001054>.
36. Yu J, Xu Q, Song JC, Li Y, Dai X, Huang DY, Zhang L, Li Y, Shi HB (2017) The value of diffusion kurtosis magnetic resonance imaging for assessing treatment response of neoadjuvant chemoradiotherapy in locally advanced rectal cancer. *Eur Radiol*. May;27(5):1848-1857. doi: <https://doi.org/10.1007/s00330-016-4529-6>.
37. Shi J, Yang S, Wang J, Huang S, Yao Y, Zhang S, Zhu W, Shao J (2019) Detecting normal pediatric brain development with diffusional kurtosis imaging. *Eur J Radiol*. Nov;120:108690. doi: <https://doi.org/10.1016/j.ejrad.2019.108690>.
38. Li L, Zhu W, Chen W, Fang J, Li J (2017) The study of the intervertebral disc microstructure in matured rats with diffusion kurtosis imaging. *Magn Reson Imaging*. Oct;42:101-106. doi: <https://doi.org/10.1016/j.mri.2017.06.010>.
39. Gao J, Feng ST, Wu B, Gong N, Lu M, Wu PM, Wang H, He X (2015) Huang B. Microstructural brain abnormalities of children of idiopathic generalized epilepsy with generalized tonic-clonic seizure: a voxel-based diffusional kurtosis imaging study. *J Magn Reson Imaging*. Apr;41(4):1088-95. doi: <https://doi.org/10.1002/jmri.24647>.
40. Luo X, Li Y, Shang Q, Liu H, Song L (2019) Role of Diffusional Kurtosis Imaging in Evaluating the Efficacy of Transcatheter Arterial Chemoembolization in Patients with Liver Cancer. *Cancer Biother Radiopharm*. Dec;34(10):614-620. doi: <https://doi.org/10.1089/cbr.2019.2878>.
41. Zhang J, Jiang J, Zhao L, Zhang J, Shen N, Li S, Guo L, Su C, Jiang R, Zhu W (2019) Survival prediction of high-grade glioma

- patients with diffusion kurtosis imaging. *Am J Transl Res.* Jun 15;11(6):3680-3688.
42. Goryawala MZ, Heros DO, Komotar RJ, Sheriff S, Saraf-Lavi E, Maudsley AA (2018) Value of diffusion kurtosis imaging in assessing low-grade gliomas. *J Magn Reson Imaging.* Dec;48(6):1551-1558. doi: <https://doi.org/10.1002/jmri.26012>.

Springer Nature or its licensor (e.g. a society or other partner) holds exclusive rights to this article under a publishing agreement with the author(s) or other rightsholder(s); author self-archiving of the accepted manuscript version of this article is solely governed by the terms of such publishing agreement and applicable law.

**Publisher's Note** Springer Nature remains neutral with regard to jurisdictional claims in published maps and institutional affiliations.